Ankle Dorsiflexion Strength Monitoring by Combining Sonomyography and Electromyography

Qiang Zhang, Zhiyu Sheng, Frank Moore-Clingenpeel, Kang Kim, Nitin Sharma

***Abstract*—Ankle dorsiflexion produced by Tibialis Anterior (TA) muscle contraction plays a significant role during human walking and standing balance. The weakened function or dysfunction of the TA muscle often impedes activities of daily living (ADL). Powered ankle exoskeleton is a prevalent technique to treat this pathology, and its intelligent and effective behaviors depend on human intention detection. A TA muscle contraction strength monitor is proposed to evaluate the weakness of the ankle dorsiflexion. The new method combines surface electromyography (sEMG) signals and sonomyography signals to estimate ankle torque during a voluntary isometric ankle dorsiflexion. Changes in the pennation angle (PA) are derived from the sonomyography signals. The results demonstrate strong correlations among the sonomyography-derived PA, the sEMG signal, and the measured TA muscle contraction force. Especially, the TA muscle strength monitor approximates the TA muscle strength measurement via a weighted summation of the sEMG signal and the PA signal. The new method shows an improved linear correlation with the muscle strength, compared to the correlations between the muscle strength and sole sEMG signal or sole PA signal, where the R-squared values are improved by 4.21 % and 1.99 %, respectively.**

I. Introduction

Ankle dorsiflexion has an essential role in both human balance control and walking [1]–[3]. The weakened function and dysfunction of foot dorsiflexion may create barriers to activities of daily living (ADL). A weakened dorsiflexion such as a drop foot may result from spinal cord injury (SCI), cerebral vascular accidents and multiple sclerosis. Powered robotic devices and functional electrical stimulation (FES) neurorehabilitation aim to induce neural reorganization through therapeutic exercises that are repeatable, flexible, and quantifiable [4]. These innovations have been used to improve weakened ankle dorsiflexion [5]–[7]. Also, to achieve better human-machine-interaction (HMI), several types of compliant actuators have been proposed to measure the HMI force [8], [9], thus to estimate human movement intention during rehabilitation. However, the ability of these therapies to strongly induce neuroplasticity and motor learning [10] depends on the measurement of weakened voluntary effort.

Voluntary effort is generated by the contraction of skeletal muscles. This muscle contraction generates architectural parameters alterations, such as pennation angle (PA) [11]–[13], fascicle length [11], [14], and muscle thickness [15], [16], in addition to active voltages at the skin surface, known as electromyography (EMG) [17]. EMG signal can be classified into surface EMG (sEMG) and intramuscular EMG (iEMG), and the difference between them is described in [18], [19]. Given the safety and convenience, currently the usage of sEMG is much more prevalent than iEMG in both clinical and research areas. A simultaneous and proportional force estimator in 2 degree-of-freedoms from iEMG was proposed in [20]. In [21], the authors found that there was a trend of better task performance with sEMG than iEMG for both able-bodied and amputee subjects. Milner-Brown et. al [22] observed that the mean rectified sEMG varied linearly with the force generated by a skeleton muscle. In [23], it was determined that an EMG-driven model could predict joint moments for a wide range of tasks and contractile conditions.

Although sEMG is easy to implement, it cannot reliably detect human intention (voluntary effort) due to its susceptibility to interference from signals coming from neighboring muscles, neither can it be used to detect deep muscle activities [21]. The authors in [24] used mechanomyography (MMG) to estimate the elbow flexion force at the waist by using an artificial neural network in comparison with sEMG. Apart from sEMG and MMG, sonomyography or ultrasound (US) imaging is another non-invasive methodology that addresses these short comings, and can be potentially used for muscle effort prediction. The architectural parameters of muscle's US images can reliably provide changes in muscle contractility of a deeply located muscle without cross-talk or interference from the adjacent muscles. As shown in [15], by comparing the architectural parameters from ultrasonographic measures (including PA, fascicle length, and muscle thickness) and EMG measures during isometric contractions over the full range of contraction intensities, the authors described the relationship between architectural parameters and EMG signal. In [12], the exponential functions between root mean square (RMS) of normalized sEMG and torque, the muscle deformation and the RMS, and the PA and the RMS were observed. In addition, the linear relationships between the

Qiang Zhang, Zhiyu Sheng, Frank Moore-Clingenpeel, Kang Kim and Nitin Sharma are with the Department of Mechanical Engineering and Materials Science, University of Pittsburgh School of Engineering, Pittsburgh, PA, USA. (e-mail: qiz81@pitt.edu, zhs41@pitt.edu, fam47@pitt.edu, kangkim@upmc.edu, and nis62@pitt.edu).

Kang Kim and Nitin Sharma are also with the Department of Bioengineering, University of Pittsburgh School of Engineering, Pittsburgh, PA, USA.Kang Kim is also with the Center for Ultrasound Molecular Imaging and Therapeutics-Department of Medicine and Heart and Vascular Institute, University of Pittsburgh School of Medicine and University of Pittsburgh Medical Center, Pittsburgh, PA, USA. Kang Kim is also with the McGowan Institute for Regenerative Medicine, University of Pittsburgh and University of Pittsburgh Medical Center, Pittsburgh, PA, USA.

This work was funded by NSF CAREER Award # 1750748.

normalized muscle deformation and torque, as well as the normalized PA and torque were observed.

As aforementioned, there are many research contributions on determining correlations among sEMG signal, architectural parameters obtained from US images of muscles, and strength or force generated by muscles. However, these studies correlate signals that are derived solely from sEMG or US images with the force generated by targeted muscles without combining sEMG and US images together. An assessment method that estimates muscle contraction strength by combining US images and sEMG signal may provide an improved performance compared to sole sEMG signal or sole US imaging signal.

The aim of this work is to investigate the feasibility of a continuous muscle strength monitor based on the model-free principle that incorporates sEMG signal and PA, detected from US images, to assess tibialis anterior (TA) muscle strength during voluntary isometric ankle dorsiflexion. The load cell signal, sEMG signal and US images are collected continuously and simultaneously from different experimental trials on an able-bodied adult participant. The correlations between sEMG signal and load cell signal, PA from US images and load cell signal, and proposed monitor and load cell signal are studied, respectively.

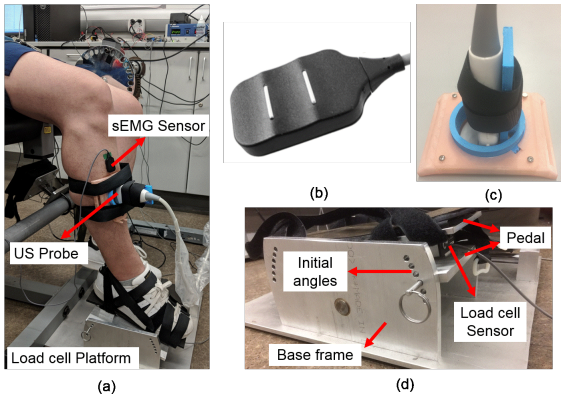

Figure 1: (a) Experimental setup employed to simultaneously record the signals from sEMG, US imaging and load cell during ankle dorsiflexion. (b) Single differential sEMG sensor. The sEMG signal is the results of the potential difference between two electrodes on the skin surface. (c) 3-D printed customized US probe holder with 1 DOF. The US probe is attached on its vertical bar and the holder is attached on the skin surface by velcro. (d) Load cell platform with 7 adjustable angular positions. The participant's foot is attached on the pedal surface

II. Methods

A. Ankle Experiments

A 27 year-old male able-bodied participant with no neuromuscular disorders was recruited for this study. The human participant experimental protocol was approved by the Institutional Review Board (IRB) at the University of Pittsburgh. The participant was briefed on the experimental procedures and volitionally signed a consent form.

The experimental setup is illustrated in Fig. 1 (a), where the participant was seated comfortably in an adjustable chair with his upper leg kept horizontal. During the experimental procedures, the participant's lower leg was restrained perpendicular to the upper leg. The load cell platform is shown in Fig. 1 (d), which includes base frame, adjustable angular positions, pedal and load cell. The angular positions of the pedal could be set as -15°, -10°, -5°, 0°, 5°, 10° and 15° corresponding to the ground. In this study, the pedal of the platform was set to be parallel to the ground by setting the initial angle to 0°. After that, both the heel and toe of the participant's foot were tied to the pedal tightly by velcro straps to guarantee the isometric ankle dorsiflexion. The load cell (MLP-300, Transducer Techniques, CA, USA) in Fig. 1 (d) was located beneath the pedal to measure the equivalent voluntary contraction force (VC) of the dorsiflexor muscle group during ankle dorsiflexion. For isometric case, the moment arm of VC was kept as a constant, and the ankle torque equaled to the multiplication of VC and moment arm. The sEMG sensor in Fig. 1 (b) (Bagnoli^{TM} Desktop, DELSYS, MA, USA) was attached to the lower leg skin through a piece of adhesive interface after shaving and cleaning with alcohol in the targeted area. A clinical linear US transducer (L7.5SC Prodigy Probe, S-Sharp, Taiwan) was pressed onto the targeted muscle of the lower leg with a special customized holder as shown in Fig. 1 (c). This holder with 1 degree of freedom (DOF) was 3-D printed, and it could adjust the orientation of the US probe from cross-sectional direction to longitudinal direction to obtain the most visualized muscle image. Conductive US gel was applied between the transducer and the skin. The transducer was placed to measure a longitudinal direction instead of a cross-sectional area. In this way inaccurate measurements due to muscle fibers moving during contraction can be avoided, because cross-sectional placement of the probe would miss the targeted area when the muscle contraction altered the location of muscle fibers.

Once the setup was initialized, the position of lower leg, the orientation of probe, and the position of the load cell platform would stay stationary until the end of experiments. Three trials were conducted, and for each trial, the duration was set to 6 seconds. The 1^{st} second was left intentionally to get US machine ready for receiving trigger signal. From the beginning of the 2^{nd} second, the US machine started to receive the trigger signal, and the participant performed ankle dorsiflexion twice within 5 seconds following a sequence including relax, maximum voluntary contraction (MVC) and relax according to oral instructions. Thus, totally there were six dorsiflexion cycles for three trials. To avoid fatiguing the muscle, a rest period of 2 minutes to 4 minutes between two trials was provided.

B. Signal Measurements and Analysis

The signal from the load cell was processed though an input signal conditioner (DRC-4710, OMEGA Engineering,

CT, USA), which amplified the original signal and filtered the noise. The signal from the sEMG sensor was processed though an input module (Bagnoli^{TM} Desktop, DELSYS, MA, USA) and a main amplifier (Bagnoli^{TM} Desktop, DELSYS, MA, USA) with a gain of 10k. In addition, the main amplifier filtered the signal to a bandwidth between 20 Hz and 450 Hz and checked for excessive amounts of line interference as well as channel clipping due to over-amplified signals. Finally, the processed load cell signal and the sEMG signal were collected by a data acquisition (DAQ) board (QPIDe Board, Quanser, Canada) through analog input channels. The signals from the US transducer were processed in an US imaging machine (Prodigy, S-Sharp, Taiwan) to image the TA muscle contraction.

Signals of sEMG, US image and load cell were synchronously recorded in a real-time system implemented in Matlab/Simulink (R2012b, MathWorks, MA, USA) controlled by trigger signals. The load cell and sEMG signals were sampled at 1000 Hz. Ultrasound imaging of 6.4 MHz center frequency with 20 frames per second in the brightness mode (B-mode) was used to scan a targeted TA muscle region. For the sEMG signal from one full contraction, the moving root mean square (MRMS) [25] [4] is given as

$$x_2(t) = rms\{l(t)\} = \left(\frac{1}{T}\int_t^{t+T} l^2(t)dt\right)^{1/2} \quad (1)$$

where $t \in \mathbb{R}$, $T \in \mathbb{R}$ and $l(t) \in \mathbb{R}$ represent the window beginning time instant, the length of the moving window, and the amplitude of sEMG signal, respectively.

Then the normalization of VC and sEMG MRMS are given

$$n_i(t) = \frac{x_i(t) - x_{i\min}}{x_{i\max} - x_{i\min}} \cdot 100\%, \quad i = 1, 2 \quad (2)$$

where $x_i(t)(i = 1, 2)$ represent VC and sEMG MRMS, respectively. $n_i(t)(i = 1, 2)$ denote the normalized values of corresponding signals. One point every 0.05 second from $n_i(t)(i = 1, 2)$ was selected to match the 20 Hz of US images, which is donated as $N_i(t)(i = 1, 2)$.

For the US images during the same contraction period collected by the commercial Prodigy software (Prodigy, S-Sharp, Taiwan) and replotted in Matlab, as shown in Fig. 2, the PA was defined as the angle between the most clearly visualized fascicle and its insertion to the deep aponeurosis surface or baseline. By subjectively drawing two lines for the fascicle and baseline in Matlab, respectively, the PA was computed through slopes of these two lines. Here, three fascicles were chosen, then the angle between each fascicle and the baseline was calculated, respectively. The average angle value was regarded as the PA for each US image.

The normalization of PA is also given as

$$N_3(t) = \frac{x_3(t) - x_{3\min}}{x_{3\max} - x_{3\min}} \cdot 100\% \quad (3)$$

where $x_3(t)$ represents PA at frame rate of 20 Hz and $N_3(t)$ denotes the normalized value of PA.

The monitoring method incorporates the normalized sEMG MRMS and PA, in the meanwhile the allocation coefficients

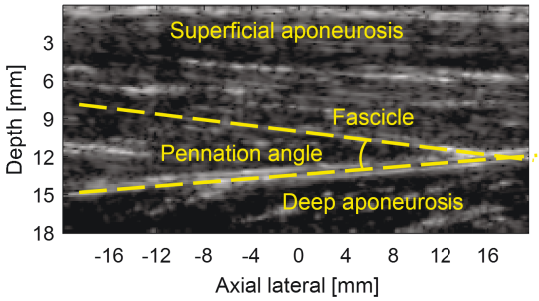

Figure 2: Pennation angle of TA muscle in US images. The angle between two dash lines is the pennation angle, and the image was taken at the moment before contraction

are set as $1 - \alpha$ and α, respectively. Then the weighted summation is given as the incorporation rule

$$N_4(t) = \alpha N_3(t) + (1 - \alpha)N_2(t) \quad (4)$$

where α is a coefficient between 0 and 1. When $\alpha = 1$ (or 0), the monitor only takes normalized PA (or sEMG MRMS) signal, otherwise, the monitor takes the weighted summation of normalized PA and normalized sEMG MRMS signals. To verify the performance of the proposed monitor, the correlations between N_1 and N_2, N_1 and N_3, as well as N_1 and N_4 were investigated by using linear regression method in Matlab. The estimated normalized VC is given as

$$\hat{f}_i = \beta_{0i} + \beta_{1i}N_i, \ i = 2, 3, 4 \quad (5)$$

where $\hat{f}_i(i = 2, 3, 4)$ denote the estimation of normalized VC by sole normalized sEMG MRMS N_2, sole normalized PA N_3 or proposed monitor N_4. β_{0i} and β_{1i} denote the y-intercepts and slopes of each linear regression, respectively. It is clear that $\hat{f}_4$ equals to $\hat{f}_2$ when α equals to 0 and $\hat{f}_4$ equals to $\hat{f}_3$ when α equals to 1.

III. Results and Discussions

A. Pre-processed Results of VC, sEMG MRMS and PA

Fig. 3 (a) shows the original measurements of the first dorsiflexion cycle in trial 1, which includes VC signal, sEMG signal and the PA signal. At the starting of the contraction, sEMG signal was the fastest one that had an obvious response, which is about 40 ms ahead of VC and PA. But there was no distinguishable time delay between VC and PA. From observing different trials, a common characteristic is found that when VC approaches to MVC very closely after 2.2 s, although VC does not have much change, the PA is still increasing, which means at the end of the contraction cycle an increasing PA will not generate more VC. This phenomenon is similar to the results as shown in [15]. The preliminary normalization results $N_i(t)(i = 1, 2, 3)$ are shown in Fig. 3 (b). In an isometric case, ankle torque equals to the multiplication of VC and the constant moment arm, so its normalization is equal to normalized VC. The sEMG MRMS can smooth the original sEMG measurement, which appears the similar functionality as a low pass filter. However,

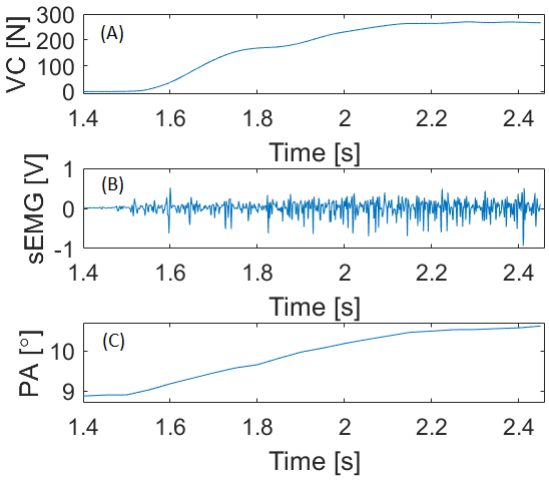

(a)

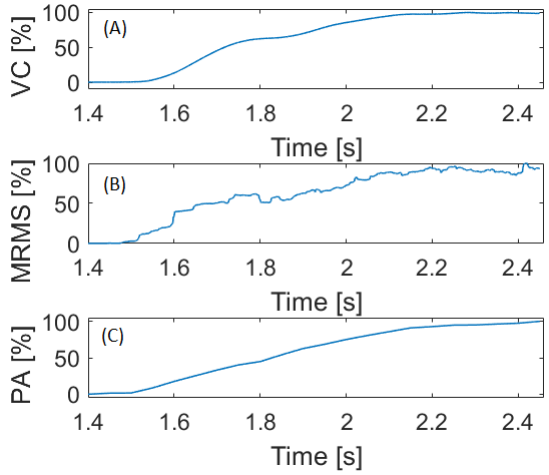

(b)

Figure 3: (a) Original measurements of VC, sEMG and PA of first dorsiflexion cycle in trial 1. During the full contraction cycle, VC in (A) and PA in (C) are increasing monotonically, and the magnitude and density of sEMG in (B) are both increasing with the increasing VC. (b) Normalized values of VC, sEMG MRMS and PA, which are denoted as N_1, N_2 and N_3, respectively, in the corresponding dorsiflexion cycle, and the feature scaling of every signal is between 0 to 100%

the smoothness and information integrity of sEMG signal are contradictory to each other, and the length of moving window in (1) affects both the smoothness and information integrity. To make a trade-off, the length of moving window was set as 0.2 second.

In Fig. 3 (a), ideally the VC was supposed to be a ramp, but since the participant performed dorsiflexion according to oral instructions, it was too difficult to maintain a strictly ramp line. The overall relationships between N_1 and N_2, N_1 and N_3 from six dorsiflexion cycles are represented as shown in Fig. 4 (a) and (b), respectively. It is obvious in Fig. 4 (b) that at the end of contraction process in each cycle, the increasing PA does not produce higher TA muscle VC. Fig 4. (a) shows

Table I: The results of linear regression between normalized VC (N_1) and normalized sEMG MRMS (N_2), normalized VC (N_1) and normalized PA (N_3)

Regression	Slopes		Y-intercepts		R^2 value	
	mean	std	mean	std	mean	std
N_1 and N_2	1.094	0.049	-11.418	2.657	0.917	0.048
N_1 and N_3	1.065	0.055	-6.807	6.773	0.954	0.041

the likely piecewise linear correlation between N_1 and N_2, whose critical point is 50% N_2, while Fig. 4 (b) shows the likely global linearity. The results of linear regression in Fig. 4 (a) and (b) are given in Table I, which includes the means and standard deviations (std) of slopes, y-intercepts and R-squared values (R^2), respectively. R^2 value is a generalized criteria to evaluate the performance of correlation. Based on R^2 values, normalized PA presents better linear correlation with normalized VC than normalized sEMG MRMS. In addition, the student's t-test shows significant difference between the two groups R^2 values (p<0.01).

B. Results of Combined sEMG MRMS and PA

From the results in Fig. 4 (a) and (b), we can infer that the combination of N_2 and N_3 is very likely to generate improved linear regression results. From the visualized US images, ideally the PA changes smoothly during the contraction, which is more reliable for indicating muscle activities than sEMG signal with embedded noise. The goal of this monitor is to reduce the error between $\hat{f}_4$ and N_1 by adjusting the allocation coefficient α compared with the error between $\hat{f}_2$ and N_1, or between $\hat{f}_3$ and N_1. Here, α is adjusted from 0 to 1 with the interval of 0.1 to get different monitoring results. To the best of our knowledge, there is no gold standard to define which linear regression should be deemed as acceptable and which one as not acceptable just based on the slopes and y-intercepts. However, in order to have a tool to draw conclusions about the significance of this work, we adopt the criterion that was used in [26] for the acceptable linear regression quality based on the R^2 values. In that study, R^2 values higher than 0.8 were a sign of acceptable estimations (the maximum value is 1). The effect of increasing α on the R^2 values between N_1 and N_4 was investigated, as shown in Fig. 5. Accordingly, all R^2 values in Fig. 5 are higher than 0.8, which indicates all linear regression operations are acceptable. Furthermore, higher R^2 means better linear regression between N_1 and N_4. The results in Fig. 5 show that in cycle 2 and 4, increasing α can generate higher R^2 and $\alpha = 1$ corresponds to maximum R^2, while in cycle 1, 3, 5 and 6 there exists an optimal α between 0.5 and 1 to maximize R^2, respectively.

To find the optimal α, the loss function, also known as error quadratic value between N_1 and $\hat{f}_4$, is defined and least mean square (LMS) algorithm is applied. The optimal α in each cycle is calculated through normal equation, which is shown in Table 2, as well as corresponded R^2 values. The optimal α in cycle 1 is smaller than any other cycles, which may result from the nonlinear and time-varying muscle

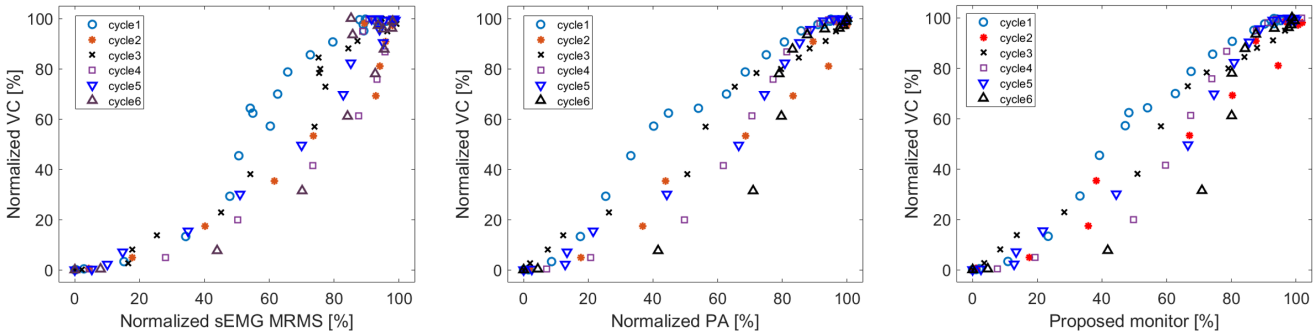

Figure 4: Typical linear regression results during one cycle of TA muscle contraction process. (a) Relationship between the normalized VC (N_1) and normalized sEMG MRMS (N_2). (b) Relationship between the normalized VC (N_1) and normalized PA (N_3). (c) Relationship between the normalized VC (N_1) and proposed monitor (N_4) with optimal α

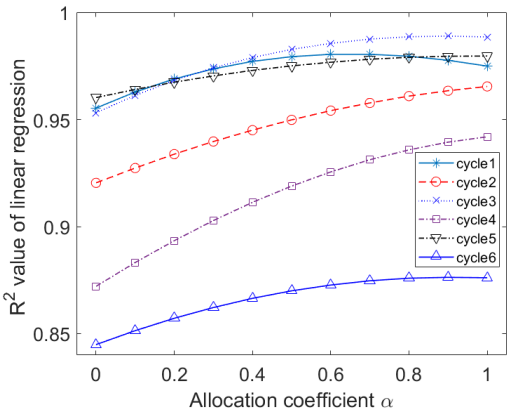

Figure 5: R^2 values in linear regression between N_1 and N_4 with increasing α, all R^2 values are higher than 0.8

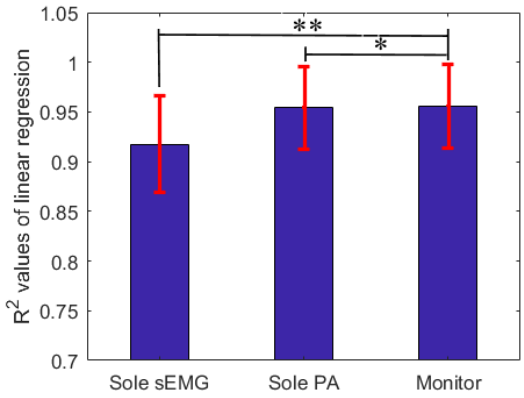

Figure 6: Mean and standard deviation of R^2 values in linear regression between N_1 and N_2, N_1 and N_3, and N_1 and N_4 with optimal α. * represents the significant difference level is at p<0.05, and ** represents the significant difference level is at p<0.01

Table II: Optimal allocation α and corresponding R^2 for the monitoring method in each dorsiflexion cycle

Cycle	1	2	3	4	5	6
Optimal α	0.653	1	0.895	1	0.983	0.915
R^2 value	0.981	0.968	0.989	0.944	0.979	0.876

dynamics. The linear regression results between N_1 and N_4 with corresponding optimal α are given in Fig. 4 (c) for six dorsiflexion cycles, where the slope is 1.075±0.054 and the y-intercept is -7.339±5.324. Compared with Fig. 4 (a) and (b), the points distribution is more concentrated, which means the monitor with optimal α has better linear correlation with VC than sole sEMG or sole PA.

Fig. 6 presents the comparison of R^2 values for the linear regression between N_1 and N_2, N_1 and N_3, and N_1 and N_4 with optimal α. Obviously, by aforementioned LMS algorithm, each α in Table II will minimize the loss function and maximize R^2 value in that cycle. The estimation $\hat{f}_4$ with optimal α improves the mean R^2 value by 4.21 % and 1.99 % than sole sEMG MRMS and sole PA, respectively. To test if there is significant improvement of R^2 value, one way ANOVA approach is used. The statistical results show significant difference for R^2 values between by sole N_2 and by N_4 (p<0.01), as well as significant difference for R^2 between by sole N_3 and by N_4 (p<0.05). These results indicate the promising functionality of the proposed monitoring method to improve the linear correlation with VC than using sole sEMG or sole PA, and better linear correlation provides the chance for guaranteeing faster muscle contraction force calculation and higher estimation accuracy.

C. Discussions

To quantitatively analyze the contraction activities of skeleton muscles, both active voltage at skin surface and architectural parameters were processed to correlate with the voluntary contraction strength in this work. The linear regression results between VC and sEMG MRMS, VC and PA, as well as VC and proposed monitor validated the effectiveness of the monitor to predict ankle dorsiflexion strength. Although sEMG signal and load cell signal could

be collected at very high frequency, the quality of US images would be deteriorated, which impedes the efficiency and accuracy of pennation angle calculation. Therefore, all results were based on the data collected at 20 Hz sampling frequency. After synthesizing six dorsiflexion cycles on this participant, in terms of linearly estimating N_1, PA has a much better performance than sEMG MRMS, as shown in Fig. 4 (a) and (b). The most possible reason arises from the piecewise linearity between N_1 and N_2 while global linearity between N_1 and N_3. On the other hand, the manually measured PA from US images in the offline manner depends on three visualized fascicles, which is subjective and may cause measurement error due to the alternative selection of fascicles. Two main challenges should be overcome before the real-time application for the proposed monitor, including before knowing the US images, it is impossible to define the fascicles, and the manual calculation of PA frame by frame is time-consuming. Future studies involving automatic fiber orientation detection algorithm are required to investigate the online VC monitoring method for real-time application. The time delay between sEMG and VC (or PA) is about 40 ms at the beginning of muscle contraction, however, due to the US images are sampled at 20 Hz, the time delay is neglected when performing linear regressions.

IV. Conclusion

This study investigated a monitoring method that combines normalized sEMG MRMS and normalized PA from US images with an allocation coefficient α to estimate voluntary TA muscle contraction strength. The strength monitor was shown to be promisingly superior to the conditions when sole sEMG signal or PA was used on an isometric dorsiflexion experiments of an able-bodied participant. The adjustment of allocation coefficient α affected the linear regression performance, and an optimal α was determined by LMS to obtain the best regression performance. The muscle strength estimation obtained from the monitor is essential for powered ankle exoskeleton or FES to achieve assist-as-needed based control strategies in rehabilitation application. In the future, more participants and more initial angular positions of the ankle will be included to verify if the proposed monitoring method can be generalized. Besides, the strategy may be implemented in a powered ankle exoskeleton.

References

[1] R. A. Mann and J. Hagy, "Biomechanics of walking, running, and sprinting," *Am J Sports Med*, vol. 8, no. 5, pp. 345–350, 1980.

[2] M. W. Cornwall and T. G. Mcpoil, "The Influence of Tibialis Anterior Muscle Activity on Rearfoot Motion during Walking," *Foot Ankle Int*, vol. 15, no. 2, pp. 75–79, 1994.

[3] M. E. Daubney and E. G. Culham, "Lower-Extremity Muscle Force and Balance Performance in Adults Aged 65 Years and Older," *Phys Ther*, vol. 79, no. 12, pp. 1177–1185, 1999.

[4] Q. Zhang, Z. S. Sheng, K. Kim, and N. Sharma, "Observer Design for a Nonlinear Neuromuscular System with Multi-rate Sampled and Delayed Output Measurements," in *Proc Am Control Conf*. Accepted, 2019.

[5] D. G. Everaert, A. K. Thompson, S. L. Su Ling Chong, and R. B. Stein, "Does Functional Electrical Stimulation for Foot Drop Strengthen Corticospinal Connections?" *Neurorehabil Neural Repair*, vol. 24, no. 2, pp. 168–177, 2010.

[6] R. van Swigchem, H. J. van Duijnhoven, J. den Boer, A. C. Geurts, and V. Weerdesteyn, "Effect of Peroneal Electrical Stimulation Versus an Ankle-Foot Orthosis on Obstacle Avoidance Ability in People With Stroke-Related Foot Drop," *Physical Therapy*, vol. 92, no. 3, pp. 398–406, 2012.

[7] J. Hausmann, C. M. Sweeney-Reed, U. Sobieray, M. Matzke, H.-J. Heinze, J. Voges, and L. Buentjen, "Functional electrical stimulation through direct 4-channel nerve stimulation to improve gait in multiple sclerosis: a feasibility study," *J Neuroeng Rehabil*, vol. 12, no. 1, p. 100, 2015.

[8] J. Sun, Z. Guo, Y. Zhang, X. Xiao, and J. Tan, "A Novel Design of Serial Variable Stiffness Actuator Based on an Archimedean Spiral Relocation Mechanism," *IEEE ASME Trans Mechatron*, vol. 23, no. 5, pp. 2121–2131, 2018.

[9] Q. Zhang, B. Xu, Z. Guo, and X. Xiao, "Design and modeling of a compact rotary series elastic actuator for an elbow rehabilitation robot," in *Proc ICIRA*, vol. 10464 LNAI. Springer, Cham, 2017, pp. 44–56.

[10] L. Marchal-Crespo and D. J. Reinkensmeyer, "Review of control strategies for robotic movement training after neurologic injury," *J Neuroeng Rehabil*, vol. 6, no. 1, p. 20, 2009.

[11] T. Fukunaga, Y. Ichinose, M. Ito, Y. Kawakami, and S. Fukashiro, "Determination of fascicle length and pennation in a contracting human muscle in vivo," *J. Appl. Physiol.*, vol. 82, no. 1, pp. 354–358, 1997.

[12] J. Shi, Y. P. Zheng, Q. H. Huang, and X. Chen, "Continuous monitoring of sonomyography, electromyography and torque generated by normal upper arm muscles during isometric contraction: Sonomyography assessment for arm muscles," *IEEE Trans Biomed Eng*, vol. 55, no. 3, pp. 1191–1198, 2008.

[13] E. M. Strasser, T. Draskovits, M. Praschak, M. Quittan, and A. Graf, "Association between ultrasound measurements of muscle thickness, pennation angle, echogenicity and skeletal muscle strength in the elderly," *AGE*, vol. 35, no. 6, pp. 2377–2388, 2013.

[14] R. L. Lieber and J. Friden, "Functional and clinical significance of skeletal muscle architecture," *Muscle & Nerve*, vol. 23, no. 11, pp. 1647–1666, 2000.

[15] P. Hodges, L. Pengel, R. Herbert, and S. Gandevia, "Measurement of muscle contraction with ultrasound imaging," *Muscle & Nerve*, vol. 27, no. 6, pp. 682–692, jun 2003.

[16] T. Abe, D. V. DeHoyos, M. L. Pollock, and L. Garzarella, "Time course for strength and muscle thickness changes following upper and lower body resistance training in men and women," *Eur. J. Appl. Physiol.*, vol. 81, no. 3, pp. 174–180, 2000.

[17] J. V. Basmajian and C. J. De Luca, *Muscles alive : their functions revealed by electromyography*. Williams & Wilkins, 1985.

[18] T. Moritani, M. Muro, and A. Nagata, "Intramuscular and surface electromyogram changes during muscle fatigue," *J. Appl. Physiol.*, vol. 60, no. 4, pp. 1179–1185, 1986.

[19] L. J. Hargrove, K. Englehart, and B. Hudgins, "A comparison of surface and intramuscular myoelectric signal classification," *IEEE Trans Biomed Eng*, vol. 54, no. 5, pp. 847–853, 2007.

[20] E. N. Kamavuako, K. B. Englehart, W. Jensen, and D. Farina, "Simultaneous and Proportional Force Estimation in Multiple Degrees of Freedom From Intramuscular EMG," *IEEE Trans Biomed Eng*, vol. 59, no. 7, pp. 1804–1807, 2012.

[21] D. L. Crouch, L. Pan, W. Filer, J. W. Stallings, and H. Huang, "Comparing Surface and Intramuscular Electromyography for Simultaneous and Proportional Control Based on a Musculoskeletal Model: A Pilot Study," *IEEE Trans Neural Syst Rehabil Eng*, vol. 26, no. 9, pp. 1735–1744, 2018.

[22] H. S. Milner-Brown and R. B. Stein, "The relation between the surface electromyogram and muscular force." *J. Physiol.*, vol. 246, no. 3, pp. 549–569, 1975.

[23] D. G. Lloyd and T. F. Besier, "An EMG-driven musculoskeletal model to estimate muscle forces and knee joint moments in vivo," *J Biomech*, vol. 36, pp. 765–776, 2003.

[24] W. Youn and J. Kim, "Estimation of elbow flexion force during isometric muscle contraction from mechanomyography and electromyography," *Med Biol Eng Comput*, vol. 48, no. 11, pp. 1149–1157, 2010.

[25] K. Watanabe and H. Akima, "Normalized EMG to normalized torque relationship of vastus intermedius muscle during isometric knee extension," *Eur. J. Appl. Physiol.*, vol. 106, no. 5, pp. 665–673, 2009.

[26] R. A. Bogey and L. A. Barnes, "An EMG-to-Force Processing Approach for Estimating in Vivo Hip Muscle Forces in Normal Human Walking," *IEEE Trans Neural Syst Rehabil Eng*, vol. 25, no. 8, pp. 1172–1179, 2017.